

pubs.acs.org/cm Article

Evaluating the Effect of Extended Conjugation and Regioisomerism on the Optoelectronic Properties and Device Efficiencies of Blue Light-Emitting Benzobisoxazoles

Published as part of Chemistry of Materials virtual special issue "In Honor of Prof. Elsa Reichmanis".

Shambhavi Tannir,* Ramiro Chavez, III, Gregorio Molina, III, Aimeé Tomlinson, and Malika Jeffries-EL*



Cite This: Chem. Mater. 2024, 36, 4945-4954



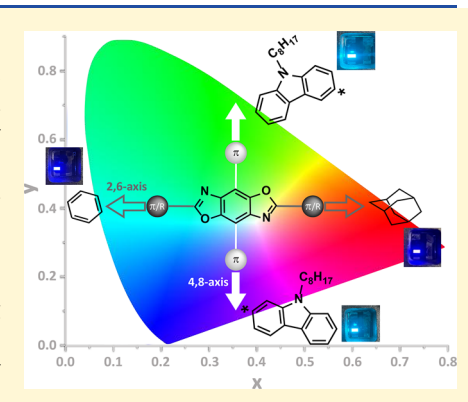
ACCESS

Metrics & More

Article Recommendations

s Supporting Information

ABSTRACT: Four new blue light-emitting materials based on benzo[1,2-d:4,5-d']bisoxazole (BBO) have been synthesized, characterized, and fabricated into organic light-emitting diode (OLED) devices. Using a combination of theoretical and experimental methods, we investigated the effect of conjugation by comparing bulky alkyl groups and planar aromatic groups along the 2,6-axis. Two of these molecules, **PB2Cz** and **PB3Cz**, are cross-conjugated cruciform-type BBOs with phenyl and carbazole groups along the 2,6 and 4,8 axes, respectively. The other two molecules, **AB2Cz** and **AB3Cz**, have extended conjugation via the carbazole groups along the 4,8-axis and bulky adamantyl groups along the 2,6-axis. Concurrently, we explored the effect of regioisomerism on optoelectronic and device properties arising from attaching carbazole at the 2- (**2Cz**) or 3- (**3Cz**) position along the 4,8-axis. The materials' geometric and electronic properties were predicted using time-dependent density functional theory (TD-DFT) calculations at the mPW3PBE/SV level. The molecules'



photoluminescent properties were measured in solution and film states. The BBO molecules were used as dopants in mixed host/guest OLED devices, producing teal to deep blue emission. Specifically, the **AB2Cz** and **AB3Cz**, with adamantyl on the 2,6-axis, exhibit blue to deep-blue emissions of 414–422 nm (CIE_x < 0.20, CIE_y < 0.10). In comparison, **PB2Cz** and **PB3Cz** have slightly longer emission wavelengths of 472–476 nm (CIE_x < 0.16, CIE_y < 0.28) and high brightness of 2700–3500 cdm⁻². The BBOs with **2Cz** resulted in more efficient devices with EQEs of ~2.8–3.2%, while the **3Cz** BBOs had EQEs of ~1.1–1.5%. This work provides insight into designing efficient, purely organic blue-fluorescent OLED materials based on the BBO moiety.

1. INTRODUCTION

Research in organic emissive materials has surged over the last few decades due to their vast applications in organic lightemitting diode (OLED) display technology, lighting, bioimaging, wearable electronics, and sensing. 1-6 Compared to conventional LEDs, OLEDs have the advantages of flexibility, lightweight, biocompatibility, low cost of production, and a wide variety of synthetic possibilities.^{7–9} The Commission Internationale de L'Eclairage (CIE) and the National Television System Committee (NTSC) define the color gamut using red, blue, and green light as the average human eye perceives. Red and green emitters have been well explored, with several recent examples showcasing excellent optoelectronic properties. However, developing efficient and stable blue-emitting materials for OLED technology remains challenging due to their high emission energies and low outcoupling efficiencies, and losses due to surface plasmons, waveguides, and substrates when in devices. 17-20 Specific applications of OLEDs, such as in visible light communications, necessitate the faster response of fluorescent OLEDs,

making blue-fluorescent emitters highly sought after.^{21–24} Applications of prompt fluorescence OLEDs also include organic pumping lasers that do not have high probabilities of electrical losses via triplet and polaron production at high charge density.^{25–27}

Organic materials are promising because their optoelectronic properties can be tuned through chemical synthesis. In addition, purely organic materials avoid using expensive rare, heavy metals such as those in phosphorescent OLEDs. However, spin statistics restrict direct fluorescence's internal quantum efficiencies (IQEs) from the singlet state (S₁) to 25%. One way to overcome the theoretical IQE is via

Received: August 18, 2023 Revised: April 22, 2024 Accepted: April 23, 2024 Published: May 9, 2024





Figure 1. (top) Schematic of BBO template; (bottom) molecular structures of the 4 BBO molecules in this work.

Table 1. Computed Structural and Optoelectronic Properties of the BBOs Conducted at the MPW3PBE/SV Level in Chloroform as a Solution Where f is the Oscillator Strength of Each System

						dihedral angles	
	HOMO (eV)	LUMO (eV)	$E_{\rm g}$ (eV)	$\lambda_{\rm abs} \ ({\rm nm})$	f	2,6	4,8
AB2Cz	-5.72	-2.67	3.05	407	1.6726		155°
AB3Cz	-5.42	-2.40	3.02	411	1.3274		156°
PB2Cz	-5.75	-2.61	2.72	456	0.9143	179°	154°
PB3Cz	-5.47	-2.47	2.58	481	0.6348	180°	153°

reversible intersystem crossing (rISC) between the S_1 and T_1 states leading to thermally activated delayed fluorescence (TADF). $^{29-32}$ For efficient TADF to occur, the $\Delta E_{(T1-T3)}$ should be < kT, which populates the T1 state. Thereafter, electrons can be transferred from the excited T_1 to the S_1 (when the E_{S1-T1} < 0.2 eV), thereby increasing the S1 population from 25 to 100% and consequently overcoming the 5% external quantum efficiency (EQE) barrier of prompt fluorescence. TADF, however, is slower than direct fluorescence and depends on a material with efficient charge transfer (CT) abilities and a high potential for triplet exciton quenching due to the long lifetimes. 33,34 Deep-blue and bluefluorescent organic emitters, such as those based on anthracene and pyrene derivatives, have also shown improved internal efficiencies beyond 25% by harnessing triplet—triplet annihilation (TTA) and their efficient spin—orbit coupling. $^{35-37}$

Our group has shown that the benzo [1,2-d:4,5-d'] bisoxazole (BBO) ring system is a versatile molecular template for designing new materials, and we have successfully tuned their optoelectronic properties by varying the groups attached at the 2,4,6, and 8 positions. Besides the ease of synthetic scalability, several BBOs have shown excellent fluorescent properties, high color purity, and thermal stability. We have previously designed deep blue and near UV light-emitting BBO

cruciforms with $^{\rm EL}\lambda_{\rm max}\approx 417$ nm; CIE $_{\rm y}<0.10.^{41,42}$ These molecules had EQEs of <1% and were theoretically limited to maximum efficiencies of 5% when considering their outcoupling and charge recombination losses. 27,43 Few highly efficient, purely organic deep-blue and blue-emitting molecules have been successfully fabricated into devices. $^{44-46}$

In this work, we have synthesized and characterized four novel BBO-based molecules functionalized by adamantane or phenyl along the 2,6-axis and carbazole along the 4,8-axis. Adamantane is a rigid, nonconjugated molecule that has been explored in hole transport materials for TADF OLEDs, and only a few examples exist of adamantane-based emitters.^{47–51} Carbazole has been widely used in emissive materials because it acts as a donor in donor-acceptor molecules. 52-54 Two of these molecules are based on the "cruciform" motif, where phenyl groups extend the conjugation along the 2,6-axis and N-octyl carbazole moieties extend it along the 4,8-axis.⁵⁵ The other two are referred to as "linear" BBOs, where the 2,6-axis is functionalized with bulky, nonconjugated adamantyl groups, and the 4,8-axis is functionalized with N-octyl carbazole groups (Figure 1). Using this series of 4 BBO molecules, we studied (i) the effect of alkyl versus aryl groups on the 2,6-axis and (ii) the impact of regioisomerism (by attaching the carbazole through the 2- or 3- position on the hydrocarbon backbone)

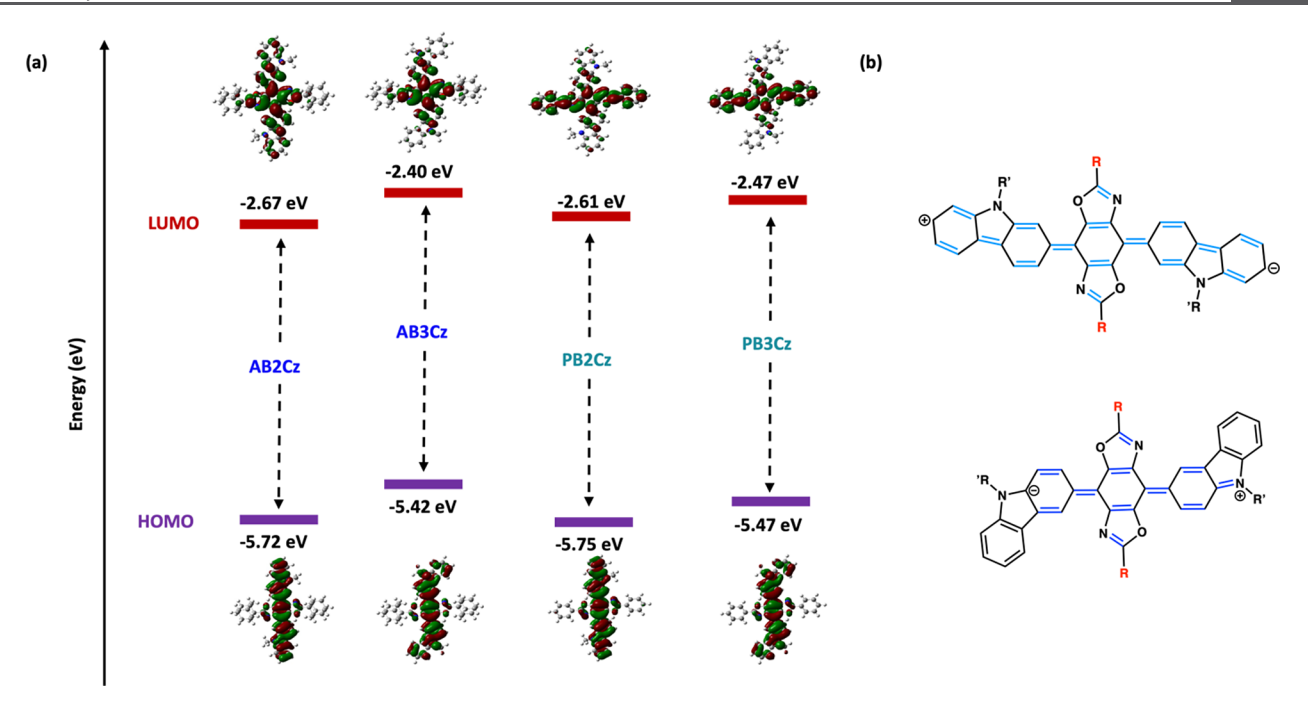


Figure 2. (a) MOs showing electron delocalization in the BBO molecules and the HOMO, LUMO, and E_g . (b) Potential conjugation pathways for the 2Cz linker (top) and the 3Cz linker (bottom). R = adamantyl or phenyl group.

Scheme 1. General Synthesis of the ABCz and PBCz Molecules

on the optoelectronic properties. We have analyzed the structure—property relationships of these molecules via photophysical, thermal, electrochemical, and computational investigations. These molecules showed promising solution state emissions, thermal stability deep-blue electroluminescence. Further, the design motif provides insight into the impact of the BBO structure and its electronic properties.

2. DENSITY FUNCTIONAL THEORY (DFT)

We used DFT calculations to aid our molecular selection and design and provide insight into their geometric and optoelectronic properties. In particular, we frequency-optimized the ground geometries of the four BBOs (Figure 1), followed by an excited state generation using TD-DFT at the mPW3PBE/SV level (see Supporting Information for details on the computational methods), a functional basis set previously benchmarked by our group. ^{41,56} Table 1 summarizes the computationally derived properties in chloroform through the conductor polarizable calculation model (CPCM), which shows the closest correlation to the experimental data; see Supporting Information for a comparison of the experimental and theoretical data in the gas phase and in chloroform. The geometric trends indicated very little difference between the carbazole linkage and the identity of

Table 2. Experimental Measurements of Electrochemical and Photophysical Properties

solution ^a								thin film ^b					
ВВО	λ_{abs} (nm)	$\begin{pmatrix} \lambda_{\mathrm{em}} \\ (\mathrm{nm}) \end{pmatrix}$	$\begin{array}{c} \varepsilon \times 10^4 \\ (\text{M}^{-1}\text{cm}^{-1}) \end{array}$	φ (%)	τ (ns)	$\begin{pmatrix} \lambda_{abs} \\ (nm) \end{pmatrix}$	$\begin{pmatrix} \lambda_{\mathrm{emis}} \\ (\mathrm{nm}) \end{pmatrix}$	$\lambda_{ m emis}$ (doped film) (nm)	φ (%)	$E_{\rm g}^{ m OPT}$ (eV)	$E_{\rm g}^{ m OPT}{ m ''}$	$HOMO^{EC}*$ (Ox^{onset}) (eV)	LUMO (eV)
AB2Cz	354	414, 438	9.9	71	1.11	371	455	414	35	2.92	3.00	-5.7 (1.3)	-2.7
AB3Cz	367	410, 430	6.6	62	1.01	358	433	422	28	2.99	3.09	-5.4 (1.0)	-2.31
PB2Cz	327, 361	452	12.6	49	1.80	337	511	478	22	2.59	2.79	-5.5(1.1)	-2.71
PB3Cz	302, 342, 357	472	12.2	53	3.52	346	518	475	26	2.56	2.72	-5.4 (1.0)	-2.58

"Measured in 1×10^{-6} M CHCl₃ solution. "Measured after spin-casting on a quartz plate (* measured after drop casting on Pt electrode). HOMO = $-4.8 + (E_{ox}^{BBO} - E_{ox}^{FC})$; LUMO; $E_g^{OPT} = 1240/\lambda_{onsev}$ thin film. $E_g^{OPT''}$ from Tauc Plot $((\alpha h v)^{1/n} \propto h v - E_g$ where h v is photon = $E_g^{OPT''} + HOMO$

energy, $E_{\rm g}$ is the energy gap, n=2 and is the power factor of transition mode), $\varphi=$ photoluminescent quantum yield; $\tau=$ lifetime.

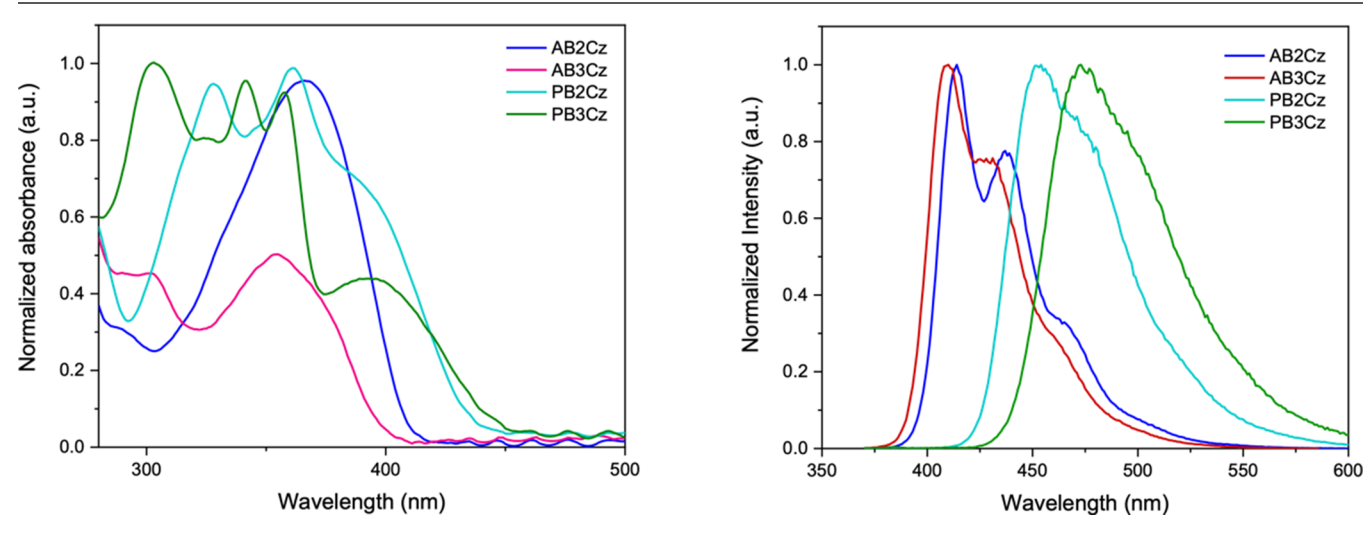


Figure 3. Absorbance (left) and emission (right) data for each BBOs in 1 μ M CHCl $_3$ solution.

the 2,6 aryl group. Therefore, all optoelectronic properties of these systems are due only to these variations and not to steric effects.

Our computations show that the highest occupied molecular orbital (HOMO) levels for the AB2Cz and PB2Cz molecules are very similar (-5.72 and -5.75 eV, respectively) and considerably lower than those of the AB3Cz and PB3Cz systems (-5.42 and -5.47 eV, respectively). These results demonstrate the significant impact the carbazole linkage position (2- or 3-) has on the HOMO levels. Additionally, the frontier molecular orbital diagrams for HOMO of the 2Cz BBOs are distributed evenly along the entire length of the 4,8axis. In contrast, in the 3Cz BBO, there is a slight localization on the terminal benzene of the linked carbazole group (Figure 2a). We hypothesized that changing the connection from the 2- to the 3- position results in two different conjugation pathways: 2Cz only has carbon atoms, whereas 3Cz has a nitrogen atom in it as illustrated in the resonance structures (Figure 2b).

We also consider the difference in properties when substituting the 2,6-axis with an alkyl (adamantyl) or aryl (phenyl) group. In the PBCz BBOs, the phenyl substitution along the 2,6-axis provides another pathway for conjugation. This leads to greater separation of the HOMO and lowest occupied molecular orbital (LUMO) levels and increased potential for intramolecular CT (Figure 2a). As the adamantyl groups do not provide an avenue for extending conjugation,

the LUMO levels are delocalized mostly along the 4,8-axis and the oxazole rings in the BBO core. The energy gaps ($E_{\rm g}$) of the ABCz-type molecules are wider (3.01–3.05 eV) than those of the PBCz BBOs (2.55–2.72 eV). Moreover, the ABCz BBOs are potentially more suitable for use as deep blue-emitting OLEDs (2.8–3.1 eV), while the PBCz BBOs emit at lower energies as predicted.

3. SYNTHESIS

The four BBOs are synthesized using a tandem approach: a condensation reaction to introduce the substituents along the 2,6-axis, followed by a cross-coupling reaction to attach the carbazole substituents at the 4,8-axis (Scheme 1). The dibromo-diamino-hydroquinone is then converted to the 2,6adamantyl or 2,6-phenyl BBO via an acid-chloride condensation. The respective 2,6-functionalized, 4,8-dibrominated BBOs are then subjected to Suzuki coupling reaction conditions with the 2- or 3-borylated carbazoles to produce the final molecules in moderate yields of 40-68%. All 4 molecules showed high thermal stability with $T_{\rm g}$ of 412 °C for AB2Cz, 387.5 °C for AB3Cz, 412.3 °C for PB2Cz, and 384.4 °C for PB3Cz, and all BBOs had melting points >300 °C. Details of each conversion and their characterizations can be found in Section 6.2. Synthesis details of the precursor molecules can be found in the Supporting Information.

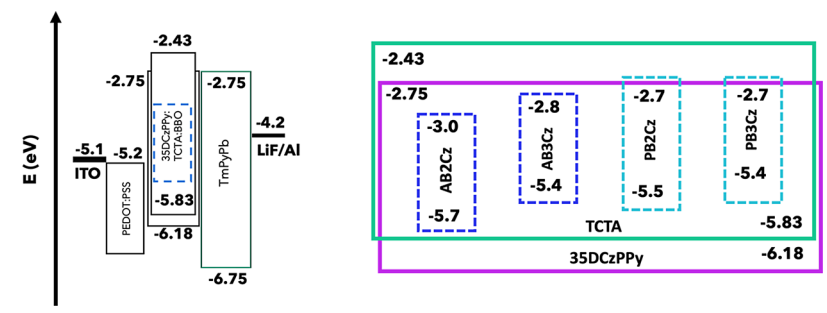


Figure 4. Energy diagram of all the device layers (left) and detailed band energies of the host–guest active layer (right). (Note – The HOMO/LUMO energies of the layers are based on those found on the website for Ossila Ltd.)

4. RESULTS AND DISCUSSION

4.1. Electrochemical Properties. The experimental electrochemical properties are included in Table 2. We used a combination of electrochemical and optical measurements to determine the HOMO, LUMO, and $E_{\rm g}$. We determined the HOMO levels from electrochemical measurements, and the $E_{\rm g}$ was calculated optical measurements (from the onset of absorption in the film and from Tauc plots). We then calculated the LUMO levels from LUMO = $E_{\rm g}$ + HOMO (Table 2). The experimental HOMO levels range from -5.3 to -5.7 eV with the same trend as that seen in the computational data, where the **2Cz** BBOs had slightly deeper HOMO levels than the **3Cz** BBOs. The experimental and theoretical HOMO levels almost match for **ABCz**, while the predicted HOMO levels of **PBCz** are 0.15-0.25 eV lower than those measured.

4.2. Photophysical/Steady-State Optical Properties. The experimental optical properties are summarized in Table 2. The solution data were measured in dilute chloroform (1 \times 10⁻⁶ M) and the thin film data on a quartz plate (Figures 3 and S8, respectively). Upon examination of the absorption curves, it is seen that the ABCz BBOs in solution and film have single peaks due to only the $\pi-\pi^*$ CT bands. The PBCz BBOs, however, show lower energy $\pi - \pi^*$ CT bands and $\mathbf{n} \cdot \pi^*$ CT bands, resulting in 2-3 strong peaks. This finding is attributed to the π - π intermolecular interactions between the 2,6-phenyl moieties. As spin-cast thin films, ABCz and PBCz materials show broad featureless peaks and bathochromic shifts of 4-10 nm in the λ_{abs} likely due to increased $\pi - \pi$ stacking in the absence of solvent. While the solution absorption data for the ABCz molecules only has one absorption peak, there is a strong emission peak ($\lambda_{\rm em}$) at approximately 412 nm and a small "shoulder" signal at 430-440 nm. PB2Cz and PB3Cz have $\lambda_{\rm em}$ of 452 and 472 nm, respectively, due to their $\pi - \pi$ interactions. The λ_{em} for ABCz in thin film is red-shifted by approximately 25 nm relative to the solution spectra. Similarly, the λ_{em} of **PBCz** is also red-shifted in thin film states, albeit to a much larger extent (20-60 nm) due to the planarity along the 2,6-axis leading to aggregation and large Stokes shifts (Figure S8). PB2Cz is red-shifted by 59 nm and PB3Cz by 46 nm, and both thin film emissions are broad, indicating a loss of resolved transitions. We also compared the PL data of each of the doped BBOs in the host (see Section 4.3 for device details) in the film state and found they have very similar emission profile shapes to the neat film state (Figure S8). The doped films, however, had narrower profiles and were less red-shifted when compared to solution emission peaks. This would be due to the lower concentration, leading to less aggregation than the neat film data. Additionally, we found emission peaks for only the BBO dopants, indicating there is no competing emission by the host materials.

The $E_{\rm g}^{\rm OPT}$ is 2.92 and 2.99 eV (when calculated from the onset of absorption) and 3.00 and 3.09 eV (when estimated from the Tauc plot) for AB2Cz and AB3Cz, respectively, which is suitable for use as deep-blue emitters. These measurements differed from the computational values by 0.13–0.21 eV (AB2Cz) and 0.02–0.11 eV (AB3Cz). The $E_{\rm g}^{\rm OPT}$ is 2.59 and 2.69 eV (when calculated from the onset of absorption) and 2.79 and 2.72 eV (when estimated from the Tauc plot) for PB2Cz and PB3Cz, respectively, indicating that their emissions would be at lower energies and, as such, they would be unlikely to produce a deep blue color.

All molecules exhibit significantly high photoluminescence quantum yields (PLQY) in solution, with the ABCz BBOs showing slightly higher PLQYs of 60–72% compared to PBCz (approximately 50%). The PBCz molecules have higher levels of intramolecular CT, as evidenced by their red-shifted broad absorption profiles and narrow $E_{\rm g}$, which is known to lower PLQYs. We explored these materials for thermally assisted delayed fluorescence. However, these systems have very short lifetimes in the nanosecond time scale, indicating they produce prompt fluorescent materials. The PBCz molecules show marginally longer lifetimes which could be due to the better separation of the FMOs along the 2,6 and 4,8 axes leading to increased intramolecular CT.

On comparing the absorption and solution data in dilute toluene (1 μ M), we found very slight differences in the λ_{max} peaks ($\Delta = 2-8$ nm) and similar profiles as those in chloroform (Figure S9). As the data for the ABCz BBOs do not show any notable changes between chloroform and toluene, the excited state transitions are due to locally excited (LE) states vs CT states. This trend is further supported by the ns lifetimes for the BBOs.

4.3. Device Properties and Discussion. Since the BBOs all showed promising $\lambda_{\rm em}$ in solution and film states, high PLQYs, and high thermal stability ($T_{\rm g} > 350$ °C, Figures S5 and S6), they were incorporated as dopants in OLEDs. We have previously reported that using a host—guest configuration for our devices⁴² as an appropriate selection of the host can suppress aggregation and improve CT between molecular species. Furthermore, we utilized a mixed host system comprising 3,5-bis(3-(carbazol-9-yl)phenyl)pyridine (35DCzPPy) and tris(4-carbazoyl-9-ylphenyl)amine (TCTA). We found that by incorporating TCTA, an electron/hole-blocking material, into the active layer, our devices showed better charge recombination and improved brightness and EQEs. 41,60,61 We used PEDOT:PSS as the hole transport material and 1,3,5-Tris(3-pyridyl-3-phenyl)benzene

Table 3. Summary of Device Properties for Each of the 4 BBOs^a

BBO	$V_{\rm on}$ (V)	drive voltage V_{100} (V)	$J_{\rm max}~({\rm mAm}^{-2})$	$L_{\rm max}~({\rm cdm^{-2}})$	CE_{max} (cdA ⁻¹)	PE_{max} (lmW^{-1})	EQE _{max} (%)	λ^{EL} (nm)	CIE 1931 (x,y)
AB2Cz	5.0	6.5	187.1	581	2.02	0.75	2.78	422.6	0.19, 0.08
AB3Cz	5.0	7.5	416.7	294	0.77	0.37	1.16	414.3	0.17, 0.08
PB2Cz	4.5	6.5	319.1	2758	3.61	1.89	3.19	476.8	0.15, 0.27
PB3Cz	3.5	5.0	413.3	3281	2.22	1.15	1.38	473.6	0.16, 0.28

 $^{a}V_{\text{on}}$ = turn-on voltage, J = current density, L = brightness, CE = current efficiency, PE = power efficiency, EQE = external quantum efficiency, and EL = electroluminescence.

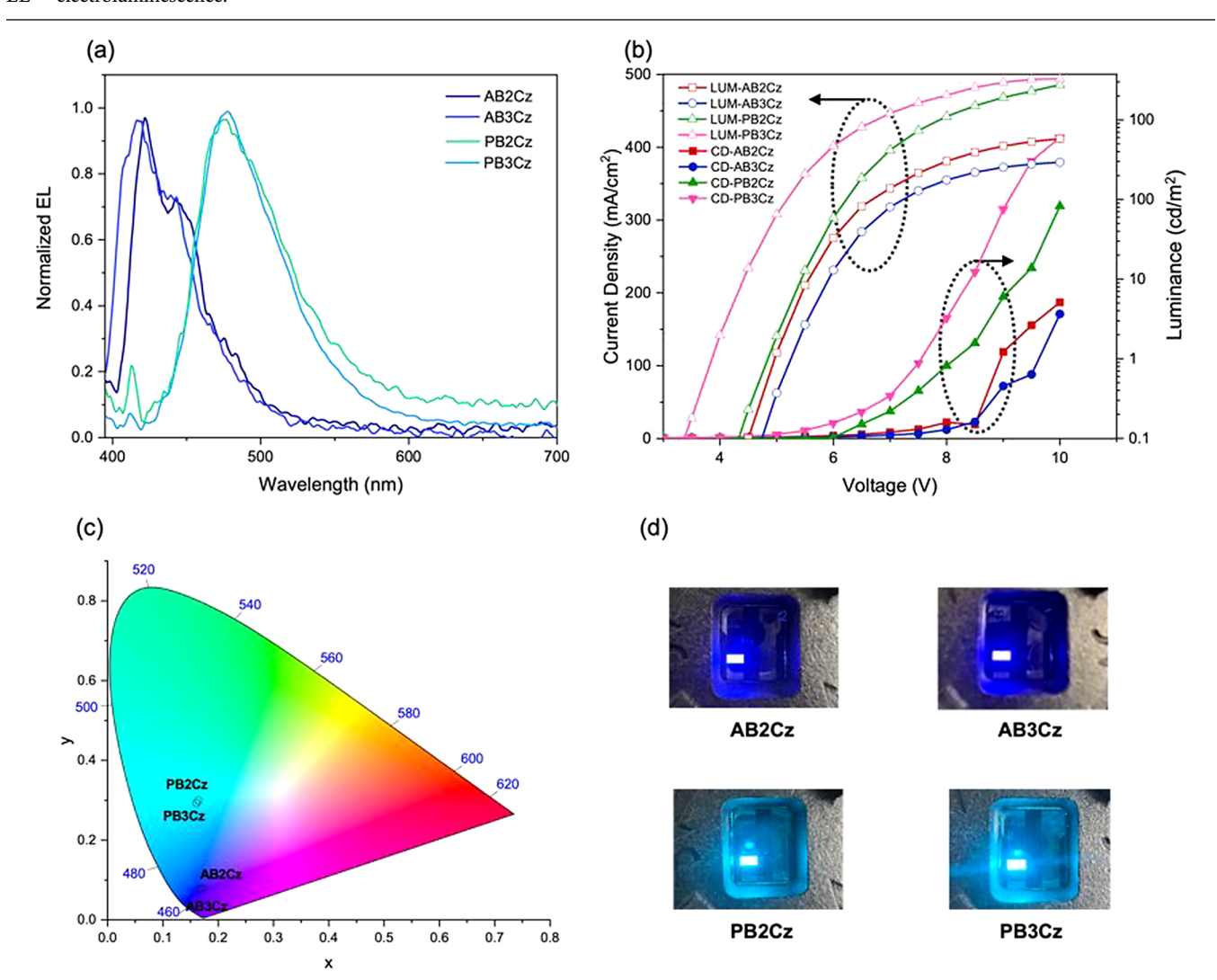


Figure 5. (a) Normalized EL spectra at 100 cdm⁻² brightness, (b) JVL curves, (c) CIE 1931 coordinates, and (d) photos of pixels of the BBOs.

(TmPyPb) as the corresponding electron transport material (Figure 4). We also tested a variety of single hosts, including poly(9-vinylcarbazole) (PVK), 1,3-Bis(N-carbazolyl)benzene (mCP), 3,3'-Di(9H-carbazol-9-yl)-1,1'-biphenyl (mCBP), 4,4'-Bis(N-carbazolyl)-1,1'-biphenyl (CBP) and TCTA as well as mixed host system of TCTA and 2,6-bis(3-(carbazol-9-yl)phenyl)pyridine (2,6DCzPPy) and found low brightness (10–1500 cd/m²) and EQEs (<0.5%) for the resulting devices. Details of the architecture and the fabrication can be found in Section 6.3.

The device properties for each of the BBO dopants (5%) can be found in Table 3. We investigated several concentrations of the AB3Cz dopant ranging from 2 to 10% and found 5% to be the most efficient (Table S1). The turn-on voltage for the ABCz molecules is expectedly higher but still at

reasonably low voltages of 5 V. In contrast, the PBCz molecules have lower turn-on voltages of 3.5–4.5 V. We see a significant difference in the brightness between the materials, with the PBCz BBOs displaying brightness of 6–10 times higher than their ABCz analogs (Figure 5). This trend is attributed to the fact that the sensor in the luminance meter is calibrated to match the spectral luminous efficiency of the human eye, which is less sensitive to deep blue colors.

Fluorescent emitters are limited to 5% EQEs when we factor in the spin statistics, outcoupling efficiencies, and recombination losses. Interestingly, the EQEs for AB2Cz and PB2Cz (2.78 and 3.19%, respectively) are much higher than those for AB3Cz and PB3Cz (1.16 and 1.38%, respectively). The devices showed EQE's \pm 0.05–0.1% and \pm 100 cd/m² for the brightness. This finding indicates that the 2-linked carbazole

has higher charge recombination efficiencies than the 3-linked carbazole, likely resulting from better HOMO-level alignment with the hosts (see Figure 4). In comparison, the 3Cz molecules could be trapping the charges, thereby lowering charge recombination. ^{62–64} We also found the EL spectra to be in good relation with the PL spectra (Figure S8).

Each of the devices described was synthesized via the solution processing method and as such do show some instabilities. We do consider the device performances of these materials to be exciting with respect to their color purity, EQEs, and brightness. However, we believe they could further be improved by employing advanced deposition techniques (such as chemical vapor deposition), which we aim to do in future research.

5. CONCLUSIONS

This work shows that we can modulate the emission color and device efficiency of BBO-based OLEDs by varying the functional groups attached along the 2,6 and 4,8 axes. The ABCz materials had a single conjugation pathway, and the PBCz molecules had two conjugation pathways, resulting in deep blue and teal emissions, respectively. Interestingly, the two regioisomers, 2Cz- and 3Cz-, resulted in different device efficiencies. The optoelectronic measurements were predicted through computation and verified experimentally. Additionally, we have successfully synthesized and fabricated 2 deep-blue, fluorescent devices based on adamantyl functionalization of the 2,6-axis, with AB2Cz and AB3Cz showing impressively deepblue coordinates CIE, of 0.08. Moreover, we have synthesized and fabricated 2 bright teal-blue devices resulting from the extended conjugation provided by phenyls on the 2,6-axis of the BBO core. Our hypothesis that shallow HOMO levels of 3linked carbazole BBOs create an injection barrier was verified in the lower EQEs of the AB3Cz and PB3Cz (1.15%). Conversely, the 2Cz BBOs had a better alignment of the HOMO levels with the host materials and showed significantly higher EQEs of 2.7-3.2% EQEs, indicating they underwent better charge recombination. These results improve our understanding of the structure-function relationships of substituted BBOs and further prove the versatility of the BBO core as a template for fluorescent emitters.

6. EXPERIMENTAL SECTION

6.1. General Methods. Details of the materials, instrumentation and analytical techniques, computational methods, and detailed synthetic procedures of the precursor molecules can be found in the Supporting Information.

6.2. General Cross-Coupling Procedure for the ABCz and PBCz Molecules via Suzuki Reaction. The substituted benzobisoxazole monomers 7 or 8 (0.25 mmol) and the corresponding boronic ester monomers 3 or 6 (0.625 mmol) were dissolved in toluene (degassed) and added to a 3-necked RBF purged with argon and fitted with a reflux condenser. One drop of Aliquot 336 (surfactant) was added to this mixture, followed by 2 M sodium carbonate (6 mL, 12 mmol). This was then deoxygenated for 30 min by pumping argon through the solution. Then the freshly prepared PEPPSI-iPr catalyst (0.0125 mmol) was added, and the reaction was kept at reflux for 36 h under argon. The reaction mixture was then diluted with chloroform and DI water. The aqueous layers were extracted thrice with chloroform (3 × 20 mL). The combined organic layers were washed sequentially with 1 M HCl (2×25 mL), DI water $(2 \times 25 \text{ mL})$, and brine $(1 \times 30 \text{ mL})$ and then dried with magnesium sulfate. The solvent was removed, and the product mixture was concentrated under pressure, and then the residue was purified by column chromatography with silica gel (gradient hexanes to 50/50 v/

v hexanes/dichloromethane). The combined eluents were concentrated under pressure, dissolved in 1.5–5 mL of chloroform, and precipitated into cold methanol ($-78\,^{\circ}$ C). The resulting powder was then passed through a second column by dry packing with silica, following the 50/50 v/v gradient, and then precipitated in methanol to yield the corresponding small molecules and used without further purification.

6.2.1. 2,6-Di(adamantan-1-yl)-4,8-bis(9-octyl-9H-carbazol-2-yl)-benzo[1,2-d:4,5-d']bis(oxazole) (AB2Cz). Monomers 3 and 7 were coupled via Suzuki cross-coupling to yield AB2Cz as a white powder (98 mg, 40% yield). ¹H NMR (400 MHz CDCl₃) δ 8.63 (2H, s), 8.31 (2H, d, J = 4 Hz), 8.27 (2H, d, J = 4 Hz), 8.15 (2H, d, J = 4 Hz), 7.48 (4H, m), 7.27 (2H, m, mixed with the CDCl3 reference peak), 4.42 (4H, t, J = 4,8 Hz), 2.31 (12H, s), 2.16 (6H, m), 2.04 (4H, p, J = 4,8 Hz), 1.87 (12H, s), 1.46 (4H, m), 1.35 (4H, m), 1.23 (12H, m), 0.83 (6H, t, J = 4,8 Hz), ¹³C NMR (500 MHz, CDCl₃) δ 173.25, 146.16, 141.48, 140.67, 137.24, 130.46, 125.85, 122.93, 122.65, 121.15, 120.69, 120.31, 118.87, 114.57, 111.13, 108.78, 77.16, 43.51, 40.59, 36.74, 36.53, 32.03, 29.72, 29.49, 29.42, 28.24, 27.74, 22.78, 14.21. HRMS (ESI) calculated for C₆₈H₇₈N₄O₂ 983.6203 [M + H]⁺; found 983.6226.

Note: $\delta_{\rm H}$ at 8.31 and 8.27 are close doublets leading to roofing.

6.2.2. 2,6-Di(adamantan-1-yl)-4,8-bis(9-octyl-9H-carbazol-3-yl)benzo[1,2-d:4,5-d']bis(oxazole) (AB3Cz). Monomers 6 and 7 were coupled via Suzuki cross-coupling to yield AB3Cz as a white powder (136 mg, 55% yield). ¹H NMR (400 MHz, CDCl₃) δ 9.22 (2H, s), 8.60 (2H, d, J = 4 Hz), 8.22 (2H, d, J = 4 Hz), 7.62 (2H, d, J = 8 Hz),7.51 (2H, t, I = 4.8 Hz), 7.46 (2H, d, I = 8 Hz, overlapping with peaks at 7.51), 7.28 (2H, t, J = 4.8 Hz, mixed with CDCl₃ reference peak), 4.38 (4H,t, J = 4, 8 Hz) 2.31-2.26 (12H, m), 1.93 (4H, m), 1.85-1.81 (16H, m), 1.55 (4H, m), 1.42 (4H, m) 1.36 (4H, m), 1.30–1.24 (12H,m) 0.87 (6H, t, J = 4.8 Hz) ¹³C NMR (500 MHz, CDCl₃) δ 173.06, 145.96, 141.03, 140.21, 136.91, 128.15, 125.73, 124.06, 123.57, 123.18, 122.46, 120.52, 119.06, 113.91, 108.96, 108.78, 77.41, 77.16, 77.16, 76.91, 43.39, 40.53, 40.32, 40.22, 40.20, 36.86, 36.77, 36.65, 36.51, 31.97, 29.58, 29.37, 29.24, 28.27, 28.14, 28.03, 27.53, 22.78, 14.23. HRMS (ESI) calculated for C₆₈H₇₈N₄O₂ 983.6203 [M + H]+; found 983.6245.

6.2.3. 4,8-Bis(9-octyl-9H-carbazol-2-yl)-2,6-diphenylbenzo[1,2-d:4,5-d']bis(oxazole) (PB2Cz). Monomers 3 and 8 were coupled via Suzuki cross-coupling to yield PB2Cz as a yellow powder (147 mg, 68% yield). ¹H NMR (400 MHz, CDCl₃) δ 8.59 (2H, s), 8.35 (6H, d, J=4 Hz), 8.31 (2H, d, J=4 Hz), 8.16 (2H, d, J=8 Hz), 7.50 (10H, m), 7.29 (2H, t, J=4,8 Hz), 4.44 (4H, t, J=4,8 Hz), 1.96 (4H, p, J=8 Hz), 1.52–1.45 (4H, m), 1.41–1.31 (4H, m), 1.28–1.17 (12H, m), 0.80 (6H, t, J=4,8 Hz) ¹³C NMR (500 MHz, CDCl₃) δ 163.45, 146.50, 141.30, 140.50, 138.52, 131.32, 129.76, 128.74, 127.60, 127.32, 125.81, 122.76, 121.12, 120.59, 120.22, 118.82, 115.05, 111.00, 108.68, 77.26, 77.00, 76.75, 43.27, 31.85, 29.56, 29.26, 29.24, 27.50, 22.59, 14.04. HRMS (ESI) calculated for C₆₀H₅₈N₄O₂ 867.4638 [M + H]⁺; found 867.4666.

6.2.4. 4,8-Bis(9-octyl-9H-carbazol-3-yl)-2,6-diphenylbenzo[1,2-d:4,5-d']bis(oxazole) (**PB3Cz**). Monomers **6** and **8** were coupled via Suzuki cross-coupling to yield **PB3Cz** as a yellow powder (133 mg, 61% yield). 1 H NMR (400 MHz, CDCl₃) δ 9.21 (2H, s), 8.60 (2H, d, J = 8 Hz), 8.40 (4H, m), 8.29 (2H, d, J = 4 Hz), 7.66 (2H, d, J = 4 Hz), 7.56-7.51 (8H, m), 7.49 (2H, d, J = 8 Hz), 7.31 (2H, t, J = 4,8 Hz), 4.40 (4H, t, J = 4,8 Hz), 1.98 (4H, J = 4,8 Hz), 1.50-1.44 (4H, m) 1.44-1.36 (4H, m) 1.32-1.27 (12H, m), 0.89 (6H, t, J = 4,8 Hz) 13 C NMR (500 MHz, CDCl₃) δ 163.59, 146.62, 141.09, 140.42, 138.51, 131.43, 129.13, 128.99, 128.31, 128.24, 127.89, 127.65, 125.89, 123.51, 123.49, 123.34, 122.61, 120.72, 119.16, 114.75, 110.15, 109.04, 108.91, 77.41, 77.36, 77.16, 76.91, 43.42, 31.99, 29.60, 29.39, 29.26, 27.55, 22.79, 14.25. HRMS (ESI) calculated for $C_{60}H_{58}N_4O_2$ 867.4638 [M + H]*; found 867.4605.

6.3. Device Fabrication. All the OLED devices were fabricated on prepatterned ITO (100 nm)/glass substrates with 20 Ω sq⁻¹ resistance (Ossila, Ltd.). They were first cleaned by sonicating in various solutions in the following order: Mucasol, water (2×), acetone, and isopropanol, and then dried in an oven for at least 1 h.

The substrates were subjected to 25 min of UV-ozone curing. Next, PEDOT:PSS (Ossila AI 4083) was spin-coated onto each substrate (3500 rpm, 2 min), followed by annealing at 120 °C for 30 min under a nitrogen atmosphere, producing an approx-35 nm layer. The active layer (conc. = 10 mgmL^{-1}) comprised a mixed host system (1:1 ratio of 35DCzPPy:TCTA) and 5% w/w dopant dissolved in chlorobenzene. The prepared solutions were allowed to stir at 50 °C overnight and filtered before solution processing. The active layer was spin-coated on top of the PEDOT:PSS at 2000 rpm for 20 s and then annealed at 180 °C for 60 min. The substrates were then transferred to a thermal evaporator, where TmPyPB (30 nm; 0.5 $\mbox{\normalfont\AA}$ s^{-1}), LiF (1 nm; 0.1 Å s^{-1}), and Al (100 nm; 2 Å s^{-1}) were sequentially evaporated at 10⁻⁶ Torr. Finally, the substrates were coated with epoxy, secured with a glass coverslip, and then cured at 365 nm for 25 min to perform measurements in ambient conditions. The electrical properties of the OLEDs were characterized using an Ossila Ltd. Lifetime System, and the electroluminescence was recorded using a Konica Minolta LS-160 luminance meter. The electroluminescent spectra were recorded using an Ocean Insight HR2000+ ES spectrometer, calibrated using a HL-3-plus light source.

ASSOCIATED CONTENT

Supporting Information

The Supporting Information is available free of charge at https://pubs.acs.org/doi/10.1021/acs.chemmater.3c02109.

Details of the materials, instruments, synthesis, photophysical properties, UV-vis, and emission data in toluene and film; cyclic voltammograms; thermogravimetric analysis and differential scanning calorimetry analysis; ¹H and ¹³C NMR spectra; atomic force microscopy images; device performance; and computational information (PDF)

AUTHOR INFORMATION

Corresponding Authors

Shambhavi Tannir — Department of Chemistry, Boston University, Boston, Massachusetts 02215, United States; orcid.org/0000-0003-3878-4798; Email: stannir4@bu.edu

Malika Jeffries-EL – Department of Chemistry and Division of Materials Science and Engineering, Boston University, Boston, Massachusetts 02215, United States; orcid.org/0000-0002-9134-4938; Email: malikaj@bu.edu

Authors

Ramiro Chavez, III — Department of Chemistry, Boston University, Boston, Massachusetts 02215, United States Gregorio Molina, III — Division of Materials Science and Engineering, Boston University, Boston, Massachusetts 02215, United States

Aimeé Tomlinson – Department of Chemistry and Biochemistry, University of North Georgia, Dahlonega, Georgia 30041, United States; © orcid.org/0000-0002-6953-4970

Complete contact information is available at: https://pubs.acs.org/10.1021/acs.chemmater.3c02109

Funding

NSF CHE-2108810.

Notes

The authors declare no competing financial interest.

ACKNOWLEDGMENTS

This article is dedicated to Elsa Reichmanis, a pioneer in the field of materials chemistry, leader in the scientific community, and a stellar role model for women. The authors thank the National Science Foundation (CHE-2108810 and CHE-2108824) and supercomputer allocation from Boston University Supercomputing Cluster for supporting this work. We also would like to thank Dr. Paul Ralifo, Dr. Norman Lee. Mr. Serge Zdanovich of the Boston University Chemistry Instrumentation Center for NMR, HR-MS, TGA/DSC access, and measurements. We thank Professor Allison Dennis for fluorimeter/integrating sphere access for quantum yield and lifetime measurements and Professor Karl Ludwig and Mr. Benli Jiang for AFM access.

ABBREVIATIONS

BBO, benzo[1,2-d:4,5-d']bisoxazole; OLED, organic lightemitting diode; EQE, external quantum efficiency; DFT, density functional theory; HOMO, highest occupied molecular orbital; LUMO, lowest occupied molecular orbital; CV, cyclic voltammetry

REFERENCES

- (1) Hsiang, E.-L.; Yang, Z.; Yang, Q.; Lan, Y.-F.; Wu, S.-T. Prospects and Challenges of Mini-LED, OLED, and Micro-LED Displays. *J. Soc. Inf. Dispersion* **2021**, 29 (6), 446–465.
- (2) Cheng, H.-B.; Li, Y.; Tang, B. Z.; Yoon, J. Assembly Strategies of Organic-Based Imaging Agents for Fluorescence and Photoacoustic Bioimaging Applications. *Chem. Soc. Rev.* **2020**, 49 (1), 21–31.
- (3) Ling, H.; Liu, S.; Zheng, Z.; Yan, F. Organic Flexible Electronics. *Small Methods* **2018**, 2 (10), No. 1800070.
- (4) Ni, F.; Li, N.; Zhan, L.; Yang, C. Organic Thermally Activated Delayed Fluorescence Materials for Time-Resolved Luminescence Imaging and Sensing. *Adv. Opt. Mater.* **2020**, 8 (14), No. 1902187.
- (5) Murawski, C.; Gather, M. C. Emerging Biomedical Applications of Organic Light-Emitting Diodes. *Adv. Opt. Mater.* **2021**, 9 (14), No. 2100269.
- (6) Garner, S.; Chowdhury, D.; Lewis, S. Ultrathin Glass Substrates for Thin, Lightweight, Flexible OLED Lighting. *Inf. Dispersion* (1975) **2019**, 35 (4), 9–13.
- (7) Yambem, S. D.; Brooks-Richards, T. L.; Forrestal, D. P.; Kielar, M.; Sah, P.; Pandey, A. K.; Woodruff, M. A. Spectral Changes Associated with Transmission of OLED Emission through Human Skin. Sci. Rep. 2019, 9 (1), 9875.
- (8) Bauri, J.; Choudhary, R. B.; Mandal, G. Recent Advances in Efficient Emissive Materials-Based OLED Applications: A Review. J. Mater. Sci. 2021, 56 (34), 18837–18866.
- (9) Song, J.; Lee, H.; Jeong, E. G.; Choi, K. C.; Yoo, S. Organic Light-Emitting Diodes: Pushing Toward the Limits and Beyond. *Adv. Mater.* **2020**, 32 (35), No. 1907539.
- (10) Fan, X.-C.; Wang, K.; Shi, Y.-Z.; Cheng, Y.-C.; Lee, Y.-T.; Yu, J.; Chen, X.-K.; Adachi, C.; Zhang, X.-H. Ultrapure Green Organic Light-Emitting Diodes Based on Highly Distorted Fused π -Conjugated Molecular Design. *Nat. Photonics* **2023**, *17* (3), 280–285.
- (11) Lucas, F.; Brouillac, C.; Fall, S.; Zimmerman, N.; Tondelier, D.; Geffroy, B.; Leclerc, N.; Heiser, T.; Lebreton, C.; Jacques, E.; et al. Simplified Green-Emitting Single-Layer Phosphorescent Organic Light-Emitting Diodes with an External Quantum Efficiency > 22%. *Chem. Mater.* **2022**, 34 (18), 8345–8355.
- (12) Rayappa Naveen, K.; Prabhu CP, K.; Braveenth, R.; Hyuk Kwon, J. Molecular Design Strategy for Orange Red Thermally Activated Delayed Fluorescence Emitters in Organic Light-Emitting Diodes (OLEDs). *Chem. Eur. J.* **2022**, 28 (12), No. e202103532.
- (13) Cui, R.; Zhou, L.; Zhao, X.; Wang, Q.; Liu, F.; Wang, J. Correction: Efficient Green Fluorescent Organic Light-Emitting

- Diodes with Extended Lifetimes by Exploiting an Iridium Complex as a Sensitizer. J. Mater. Chem. C 2022, 10 (2), 774.
- (14) Lu, G.; Wu, R.; Li, N.; Wang, X.; Zhou, L.; Yang, C. Naphthyridine-Based Iridium(Iii) Complexes for Green to Red OLEDs with EQEs over 30% and Low Efficiency Roll-Off. *J. Mater. Chem. C* **2022**, *10* (45), 17303–17308.
- (15) Jiang, R.; Wu, X.; Liu, H.; Guo, J.; Zou, D.; Zhao, Z.; Tang, B. Z. High-Performance Orange—Red Organic Light-Emitting Diodes with External Quantum Efficiencies Reaching 33.5% Based on Carbonyl-Containing Delayed Fluorescence Molecules. *Adv. Sci.* 2022, 9 (3), No. 2104435.
- (16) Lee, D. R.; Kim, B. S.; Lee, C. W.; Im, Y.; Yook, K. S.; Hwang, S.-H.; Lee, J. Y. Above 30% External Quantum Efficiency in Green Delayed Fluorescent Organic Light-Emitting Diodes. *ACS Appl. Mater. Interfaces* **2015**, 7 (18), 9625–9629.
- (17) Ahn, D. H.; Kim, S. W.; Lee, H.; Ko, I. J.; Karthik, D.; Lee, J. Y.; Kwon, J. H. Highly Efficient Blue Thermally Activated Delayed Fluorescence Emitters Based on Symmetrical and Rigid Oxygen-Bridged Boron Acceptors. *Nat. Photonics* **2019**, *13* (8), 540–546.
- (18) Song, W.; Lee, J. Y. Degradation Mechanism and Lifetime Improvement Strategy for Blue Phosphorescent Organic Light-Emitting Diodes. *Adv. Opt. Mater.* **2017**, *5* (9), No. 1600901.
- (19) Sarma, M.; Wong, K.-T. Development of Materials for Blue Organic Light Emitting Devices. *Chem. Rec.* **2019**, 19 (8), 1667–1692.
- (20) Brütting, W.; Frischeisen, J.; Schmidt, T. D.; Scholz, B. J.; Mayr, C. Device Efficiency of Organic Light-Emitting Diodes: Progress by Improved Light Outcoupling. *Phys. status solidi* **2013**, 210 (1), 44–65.
- (21) López-Fraguas, E.; Arredondo, B.; Vega-Colado, C.; Pozo, G. del; Najafi, M.; Martín Martín, D.; Galagan, Y.; Sánchez Pena, J. M.; Vergaz, R.; Romero, B. Visible Light Communication System Using an Organic Emitter and a Perovskite Photodetector. *Org. Electron.* **2019**, 73, 292–298.
- (22) Guo, K.; Tang, Z.; Chou, X.; Pan, S.; Wan, C.; Xue, T.; Ding, L.; Wang, X.; Huang, J.; Zhang, F.; et al. Printable Organic Light-Emitting Diodes for next-Generation Visible Light Communications: A Review. *Adv. Photonics Nexus* **2023**, 2 (4), No. 044001.
- (23) Chaleshtori, Z. N.; Chvojka, P.; Zvanovec, S.; Ghassemlooy, Z.; Haigh, P. A. A Survey on Recent Advances in Organic Visible Light Communications. In 2018 11th International Symposium on Communication Systems, Networks & Digital Signal Processing (CSNDSP); 2018; pp 1–6.
- (24) Yoshida, K.; Manousiadis, P. P.; Bian, R.; Chen, Z.; Murawski, C.; Gather, M. C.; Haas, H.; Turnbull, G. A.; Samuel, I. D. W. 245 MHz Bandwidth Organic Light-Emitting Diodes Used in a Gigabit Optical Wireless Data Link. *Nat. Commun.* 2020, 11 (1), 1171.
- (25) Chénais, S.; Forget, S. Recent Advances in Solid-State Organic Lasers. *Polym. Int.* **2012**, *61* (3), 390–406.
- (26) Zhang, Q.; Tao, W.; Huang, J.; Xia, R.; Cabanillas-Gonzalez, J. Toward Electrically Pumped Organic Lasers: A Review and Outlook on Material Developments and Resonator Architectures. *Adv. Photonics Res.* **2021**, 2 (5), No. 2000155.
- (27) Shukla, A.; Hasan, M.; Banappanavar, G.; Ahmad, V.; Sobus, J.; Moore, E. G.; Kabra, D.; Lo, S.-C.; Namdas, E. B. Controlling Triplet—Triplet Upconversion and Singlet-Triplet Annihilation in Organic Light-Emitting Diodes for Injection Lasing. *Commun. Mater.* 2022, 3 (1), 27.
- (28) Yao, L.; Yang, B.; Ma, Y. Progress in Next-Generation Organic Electroluminescent Materials: Material Design beyond Exciton Statistics. *Sci. China Chem.* **2014**, *57* (3), 335–345.
- (29) Zhang, Q.; Li, J.; Shizu, K.; Huang, S.; Hirata, S.; Miyazaki, H.; Adachi, C. Design of Efficient Thermally Activated Delayed Fluorescence Materials for Pure Blue Organic Light Emitting Diodes. *J. Am. Chem. Soc.* **2012**, *134* (36), 14706–14709.
- (30) Chen, X. K.; Kim, D.; Brédas, J. L. Thermally Activated Delayed Fluorescence (TADF) Path toward Efficient Electroluminescence in Purely Organic Materials: Molecular Level Insight. Acc. Chem. Res. 2018, 51 (9), 2215–2224.

- (31) Naveen, K. R.; Palanisamy, P.; Chae, M. Y.; Kwon, J. H. Multiresonant TADF Materials: Triggering the Reverse Intersystem Crossing to Alleviate the Efficiency Roll-off in OLEDs. *Chem. Commun.* **2023**, *59* (25), 3685–3702.
- (32) Zhao, G.; Liu, D.; Wang, P.; Huang, X.; Chen, H.; Zhang, Y.; Zhang, D.; Jiang, W.; Sun, Y.; Duan, L. Exceeding 30% External Quantum Efficiency in Non-Doped OLEDs Utilizing Solution Processable TADF Emitters with High Horizontal Dipole Orientation via Anchoring Strategy. *Angew. Chem., Int. Ed.* **2022**, *61* (45), No. e202212861.
- (33) Hasan, M.; Shukla, A.; Mamada, M.; Adachi, C.; Lo, S.-C.; Namdas, E. B. Correlating Exciton Dynamics of Thermally Activated Delayed-Fluorescence Emitters to Efficiency Roll-Off in OLEDs. *Phys. Rev. Appl.* **2022**, *18* (5), No. 054082.
- (34) Jinnai, K.; Nishimura, N.; Adachi, C.; Kabe, R. Thermally Activated Processes in an Organic Long-Persistent Luminescence System. *Nanoscale* **2021**, *13* (18), 8412–8417.
- (35) Jiang, H.; Tao, P.; Wong, W.-Y. Recent Advances in Triplet—Triplet Annihilation-Based Materials and Their Applications in Electroluminescence. *ACS Mater. Lett.* **2023**, 5 (3), 822–845.
- (36) Lim, H.; Woo, S.-J.; Ha, Y. H.; Kim, Y.-H.; Kim, J.-J. Breaking the Efficiency Limit of Deep-Blue Fluorescent OLEDs Based on Anthracene Derivatives. *Adv. Mater.* **2022**, *34* (1), No. 2100161.
- (37) Yang, G.-X.; Liu, D.-H.; Gu, Q.; Peng, X.; Li, D.-L.; Li, M.; Liu, M.; Chen, J.; Liu, K.; Su, S.-J. Triplet—Triplet Annihilation Enhanced Deep-Blue Organic Light-Emitting Diodes by Naphtho[1,2-d]-Imidazole-Isomer Derivatives with Spin—Orbit Coupling. *Adv. Opt. Mater.* **2023**, *11* (18), No. 2300455.
- (38) Burney-Allen, A. A.; Shaw, J.; Wheeler, D. L.; Diodati, L.; Duzhko, V.; Tomlinson, A. L.; Jeffries-El, M. Benzobisoxazole Cruciforms: A Cross-Conjugated Platform for Designing Tunable Donor/Acceptor Materials. *Asian J. Org. Chem.* **2020**, *10*, 215–223.
- (39) Chavez, R., III; Cai, M.; Tlach, B.; Wheeler, D. L.; Kaudal, R.; Tsyrenova, A.; Tomlinson, A. L.; Shinar, R.; Shinar, J.; Jeffries-EL, M. Benzobisoxazole Cruciforms: A Tunable, Cross-Conjugated Platform for the Generation of Deep Blue OLED Materials. *J. Mater. Chem. C* **2016**, *4* (17), 3765–3773.
- (40) Speetzen, E. D.; Shinar, R.; Jeffries-el, M.; et al. Investigating the Impact of Conjugation Pathway on the Physical and Electronic Properties of Benzobisoxazole-Containing Polymers. *J. Mater. Chem.* C 2017, 5, 12839–12847.
- (41) Wheeler, D. L.; Tannir, S.; Smith, E.; Tomlinson, A. L.; Jeffries-EL, M. A Computational and Experimental Investigation of Deep-Blue Light-Emitting Tetraaryl-Benzobis[1,2-d:4,5-d']Oxazoles. *Mater. Adv.* 2022, 3, 3842–3852.
- (42) Wheeler, D. L.; Fisher, Jr; Friederich, P.; Cunningham, C.; et al. Carbazole-Substituted Benzobisoxazoles: Near-UV Fluorescent Emitters and Ambipolar Hosts for Organic Light-Emitting Diodes. *J. Mater. Chem. C* **2023**, *11*, 211–222.
- (43) Kondakov, D. Y. Triplet—Triplet Annihilation in Highly Efficient Fluorescent Organic Light-Emitting Diodes: Current State and Future Outlook. *Philos. Trans. R. Soc., A* **2015**, 373 (2044), 20140321.
- (44) Monkman, A. Why Do We Still Need a Stable Long Lifetime Deep Blue OLED Emitter? *ACS Appl. Mater. Interfaces* **2022**, *14* (18), 20463–20467.
- (45) Cheon, H.-J.; Woo, S.-J.; Baek, S.-H.; Lee, J.-H.; Kim, Y.-H. Dense Local Triplet States and Steric Shielding of a Multi-Resonance TADF Emitter Enable High-Performance Deep-Blue OLEDs. *Adv. Mater.* **2022**, 34 (50), No. 2207416.
- (46) Hwang, J.; Koh, C. W.; Ha, J. M.; Woo, H. Y.; Park, S.; Cho, M. J.; Choi, D. H. Aryl-Annulated [3,2-a] Carbazole-Based Deep-Blue Soluble Emitters for High-Efficiency Solution-Processed Thermally Activated Delayed Fluorescence Organic Light-Emitting Diodes with CIEy < 0.1. ACS Appl. Mater. Interfaces 2021, 13 (51), 61454–61462. (47) Gu, Y.; Zhou, X.; Li, Y.; Wu, K.; Wang, F.; Huang, M.; Guo, F.;
- (47) Gu, Y.; Zhou, X.; Li, Y.; Wu, K.; Wang, F.; Huang, M.; Guo, F.; Wang, Y.; Gong, S.; Ma, D.; et al. Tetrasubstituted Adamantane Derivatives with Arylamine Groups: Solution-Processable Hole-Transporting and Host Materials with High Triplet Energy and

- Good Thermal Stability for Organic Light-Emitting Devices. *Org. Electron.* **2015**, 25, 193–199.
- (48) Zhang, K.; Wang, L.; Liang, Y.; Yang, S.; Liang, J.; Cheng, F.; Chen, J. A Thermally and Electrochemically Stable Organic Hole-Transporting Material with an Adamantane Central Core and Triarylamine Moieties. *Synth. Met.* **2012**, *162* (5), 490–496.
- (49) Guan, H.-M.; Hu, Y.-X.; Xiao, G.-Y.; He, W.-Z.; Chi, H.-J.; Lv, Y.-L.; Li, X.; Zhang, D.-Y.; Hu, Z.-Z. Novel Adamantane-Bridged Phenanthroimidazole Molecule for Highly Efficient Full-Color Organic Light-Emitting Diodes. *Dye. Pigment.* **2020**, *177*, No. 108273.
- (50) Ma, Z.; Dong, W.; Hou, J.; Duan, Q.; Shao, S.; Wang, L. Dendritic Host Materials with Non-Conjugated Adamantane Cores for Efficient Solution-Processed Blue Thermally Activated Delayed Fluorescence OLEDs. J. Mater. Chem. C 2019, 7 (38), 11845–11850.
- (51) Gu, Y.; Zhu, L.; Li, Y.; Yu, L.; Wu, K.; Chen, T.; Huang, M.; Wang, F.; Gong, S.; Ma, D.; et al. Adamantane-Based Wide-Bandgap Host Material: Blue Electrophosphorescence with High Efficiency and Very High Brightness. *Chem. Eur. J.* 2015, 21 (22), 8250–8256.
- (52) Nakanotani, H.; Higuchi, T.; Furukawa, T.; Masui, K.; Morimoto, K.; Numata, M.; Tanaka, H.; Sagara, Y.; Yasuda, T.; Adachi, C. High-Efficiency Organic Light-Emitting Diodes with Fluorescent Emitters. *Nat. Commun.* **2014**, *5* (1), 4016.
- (53) Kim, M.; Jeon, S. K.; Hwang, S.-H.; Lee, J. Y. Stable Blue Thermally Activated Delayed Fluorescent Organic Light-Emitting Diodes with Three Times Longer Lifetime than Phosphorescent Organic Light-Emitting Diodes. *Adv. Mater.* **2015**, 27 (15), 2515—2520.
- (54) Uoyama, H.; Goushi, K.; Shizu, K.; Nomura, H.; Adachi, C. Highly Efficient Organic Light-Emitting Diodes from Delayed Fluorescence. *Nature* **2012**, *492* (7428), 234–238.
- (55) Chavez, R.; Diodati, L.; Wheeler, D. L.; Shaw, J.; Tomlinson, A. L.; Jeffries-EL, M. Evaluating the Impact of Fluorination on the Electro-Optical Properties of Cross-Conjugated Benzobisoxazoles. *J. Phys. Chem. A* **2019**, *123* (7), 1343–1352.
- (56) Tomlinson, L.; Jeffries-EL, M.; Wheeler, D. L.; Diodati, A. V. Evaluating the Role of Molecular Heredity in the Optical and Electronic Properties of Cross-Conjugated Benzo[1,2-d:4,5-d']-Bisoxazoles. ACS Omega 2020, 5, 12374 DOI: 10.1021/acsomega.0c01126.
- (57) Pertegás, A.; Wong, M. Y.; Sessolo, M.; Zysman-Colman, E.; Bolink, H. J. Efficient Light-Emitting Electrochemical Cells Using Small Molecular Weight, Ionic, Host-Guest Systems. *ECS J. Solid State Sci. Technol.* **2016**, *S* (1), R3160.
- (58) Kawamura, Y.; Brooks, J.; Brown, J. J.; Sasabe, H.; Adachi, C. Intermolecular Interaction and a Concentration-Quenching Mechanism of Phosphorescent Ir(III) Complexes in a Solid Film. *Phys. Rev. Lett.* **2006**, *96* (1), No. 017404.
- (59) Zhang, Y. Q.; Zhong, G. Y.; Cao, X. A. Concentration Quenching of Electroluminescence in Neat Ir(Ppy)3 Organic Light-Emitting Diodes. *J. Appl. Phys.* **2010**, *108* (8), No. 083107.
- (60) Kumar, M.; Pereira, L. Mixed-Host Systems with a Simple Device Structure for Efficient Solution-Processed Organic Light-Emitting Diodes of a Red-Orange TADF Emitter. ACS Omega 2020, 5 (5), 2196–2204.
- (61) Jiang, Z.-L.; Tian, W.; Kou, Z.-Q.; Cheng, S.; Li, Y.-H. The Influence of the Mixed Host Emitting Layer Based on the TCTA and TPBi in Blue Phosphorescent OLED. *Opt. Commun.* **2016**, 372, 49–52
- (62) Yimer, Y. Y.; Bobbert, P. A.; Coehoorn, R. Charge Transport in Disordered Organic Host-Guest Systems: Effects of Carrier Density and Electric Field. *J. Phys.: Condens. Matter* **2008**, 20 (33), No. 335204.
- (63) Li, P.; Lu, Z.-H. Interface Engineering in Organic Electronics: Energy-Level Alignment and Charge Transport. *Small Sci.* **2021**, *1* (1), No. 2000015.
- (64) Li, P.; Lu, Z.-H. Charge-Transport Processes in Host-Dopant Organic Semiconductors. *Adv. Electron. Mater.* **2020**, *6* (3), No. 1901147.